Journal of Constructional Steel Research 172 (2020) 106200

Contents lists available at ScienceDirect

Journal of Constructional Steel Research

Fatigue crack repair in welded structures via tungsten inert gas remelting and high frequency mechanical impact

Hassan Al-Karawi [a,*,1], R.U. Franz von Bock und Polach [b], Mohammad Al-Emrani [a]

[a] Department of Architecture and Civil Engineering, Chalmers University of Technology, Sweden
[b] Institute for Ship Structural Design and Analysis, Hamburg University of Technology, Germany

ARTICLE INFO

Article history:
Received 23 April 2020
Received in revised form 30 May 2020
Accepted 2 June 2020
Available online xxxx

Keywords:
High frequency mechanical impact
TIG remelting
Crack repair
Crack retrofitting
Life extension
Pre-fatigue

ABSTRACT

Rehabilitation of welded structures has gained increasing attention lately. This paper aims at investigating the efficiency of Tungsten Inert Gas (TIG)-remelting and TIG-remelting followed by High Frequency Mechanical Impact treatment (TIG-HFMI) in fatigue life extension. Fatigue tests were carried out on as-welded and cracked specimens after treatment. The lives of the treated specimens increased remarkably by the two methods (TIG and TIG-HFMI). Many of the treated specimens ran-out after *10* million cycles of loading and failed at the clamping location when tested at a higher stress range. The improvement in compressive residual stresses, hardness values and weld toe radii were the reasons behind the life extension. These factors were used for fatigue life estimation in as-welded and TIG-treated specimens using the base metal S—N curve. Moreover, the test results together with results from previous tests in the literature demonstrated that these methods can be useful for crack retrofitting as for new structures.

1. Introduction

One of the major challenges facing the durability of steel structures is the fatigue of their welded details due to cyclic loading. These details are more prone to fatigue than other parts of the structure because of their higher susceptibility to cracks. Fatigue in welds can be traced back to three reasons: the tensile welding residual stress, the high stress concentration at the toe and the presence of different forms of weld defects (e.g. undercut) [1]. Several post-weld treatment methods have been proposed in the literature to extend the life of the welds and increase their fatigue strength. These methods can be branched into two categories based on their effect:weld geometry improvers (such as TIG-remelting or burr-grinding) which mainly aim to reduce the stress concentration factor, and residual stress improvers (such as peening or stress relief) which aim to eliminate the tensile residual stress or induce compressive residual stress. The International Institute of Welding (IIW) reported a *30%* increase in fatigue strength after TIG-remelting without altering the slope of the S—N curve [2]. On the other hand, peening was reported to increase the fatigue strength furthermore and reduce the slope of the S—N curve of the detail [3].

TIG remelting aims to eliminate the weld flaws through fusing the material at the weld toe by the local heat input. In addition, it provides smooth transition between the weld and the main plate which reduces the local stress concentration. Several studies established the benefit of TIG-remelting in enhancing the fatigue strength of new structures [4–11]. Pedersen et al. concluded that TIG-remelting is the best studied treatment method for implementation in mass production. Lieurade et al. found that treating butt and cruciform welded joints with TIG-melting resulted in fatigue strength improvement of steels with different qualities [12]. Moreover, Lixing et al. studied the performance of TIG-treated joints under constant and variable amplitude loadings, it was concluded that the improvement in fatigue strength is approximately the same under both loading conditions [13].

Few research effort projects were conducted to study the efficiency of TIG-remelting in fatigue crack repair. [14–17]. TIG remelting effect on cracked T-joint was studied by Ramalho et al. and it was found that the treatment is capable of extending the fatigue life by a factor of 2.5 [15]. Besides, the effect of crack size in cover plate details treated by TIG-remelting was studied by Fisher et.al [16,18]; they found that cracks initiated from weld root which demonstrates the significant enhancement in fatigue strength of the weld toe. In additions, TIG remelting was found to be the best of the three studied methods. Baumgartner et al. concluded that TIG-treatment can trigger crack initiation in different location such as base metal and weld roots [19]. Miki et.al concluded -after studying both transverse and longitudinal attachment details- that the life extension depends on the crack depth before treatment and TIG fusion depth [14].

High Frequency Mechanical Impact (HFMI) is one of the newest and most promising treatment method. This method is given in the literature by different names: Hammer peening, Ultrasonic impact treatment,

* Corresponding author.
E-mail address: hassan.alkarawi@chalmers.se (H. Al-Karawi).
[1]Full postal address: Västra Andersgårdsgatan 15A, Lgh 1102, 41,715, Göteborg, Sweden

https://doi.org/10.1016/j.jcsr.2020.106200

Nomenclature

$\Delta\sigma$	applied stress range
$\Delta\sigma_{EQV}$	equivalent stress range
$\Delta\sigma_{ar}$	fully reversed stress range
$\Delta\sigma_l$	local notch stress range
$\Delta\sigma_g$	nominal applied stress range
$\sigma_{m,\,g}$	nominal mean stress
$\sigma_{m,\,l}$	local notch mean stress
$\sigma_{u,\,g}$	tensile strength of S355 steel
$\sigma_{u,\,l}$	local notch tensile strength
σ_{RS}	residual stress at the weld toe
σ_{clamp}	clamping stress at the weld toe
K_t	stress concentration factor
A, B	Basquin's equations constancts
$N_{f,\,calc}$	calculated number of cycles to failure
$N_{f,\,exp}$	obtained number of cycles to failure from tests
ϕ	distortion angle
m	slope of the S—N curve
N_f	number of cycles

Abbreviations

F	weld toe failure
CF	failure at the clamping position
RO	run-out
TIG	tungsten inert gas
HFMI	high frequency mechanical impact treatment
IIW	international institute of welding
FAT	fatigue strength class

Ultrasonic needle peening and HiFIT. HFMI has a triple beneficial effect on welds; it induces compressive residual stress at the weld toe and contributes in local material hardening. In additions, it reduces the stress concentration locally [20]. HFMI has been used extensively in the literature for repairing cracked structures [21–31]. Unlike TIG-remelting, HFMI causes crack closure and does not remove the crack completely [20]. Nonetheless, combining TIG-remelting with HFMI-treatment causes crack removal and introduces compressive residual stress. This combination was found to be superior to the individual TIG or HFMI treatment of welds [9,32,33]. However, TIG-HFMI treatment has not -to the best of the author's knowledge- been investigated as a crack retrofitting method in the literature.

There is no consensus in the literature on the allowable crack size which can be removed by TIG-remelting; this is attributed to the variability in crack detection methods, fusion depths, detail types, heat inputs and applied loading levels. However, A common conclusion was found in the literature about fusion depth which should be always greater than existing crack depth to give satisfactory results [14]. This necessitates the use of relatively precise crack detection methods and ensuring the fusion depth regularity over the treated area [34].

TIG remelting requires highly skilled labor which explains its scarcity in the literature for crack retrofitting. In addition, there is no available knowledge on the use of TIG-HFMI treatment in repairing fatigue cracks. Therefore, this paper presents some fatigue test results and several experimental investigations on the efficiency of these two methods in fatigue crack repair and shed the light on the factors behind life extension. Moreover, a simple calculation tool based on Basquin's Equation is used to incorporate these factors to predict the fatigue life of the treated specimens. A special light will be thrown on comparing the strength of the treated new and cracked structures.

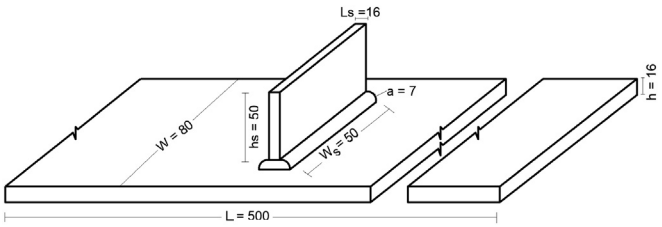

Fig. 1. The studied specimens geometry (dimensions in mm).

Table 1
The chemical composition and the mechanical properties of S355 and C6LF filler [37].

		Chemical composition				
		C	Si	Mn	S	P
S355	%	0.23	0.05	1.6	0.05	0.05
C6LF	%	0.03	0.73	1.51	0.01	0.01

	Mechanical properties		
	Yield strength MPa	Ultimate strength MPa	Elongation %
S355	355	575	22
C6LF	462	538	30

Table 2
Welding parameters.

Run	Current A	Voltage V	Speed mm/s	Heat input KJ/mm
1	240	28.3	5.8	0.9
2	235	28.3	5.6	0.95

2. Testing program

2.1. Test specimens and materials

In light of the literature review, fatigue testing program was set up consisting of 27 transverse attachment specimens. The dimensions of the specimen are given in Fig. 1. The specimens were made of mild steel S355. The welding filler material was made of core weld C6LF (metal cored wire). The chemical composition and the mechanical properties of the steel and the filler material are listed in Table 1. The properties and the compositions were obtained from the materials certificates [35,36].

2.2. Welding and fabrication

Metal active gas welding with a Mison 18 shielding gas were used to join the attachment and the base plate. The attachments were prepared

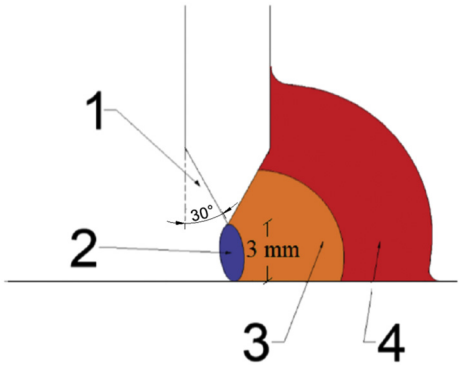

Fig. 2. Welding procedures: 1: Machining the stiffener. 2: Tack welding. 3: Root welding. 4: Cap welding.

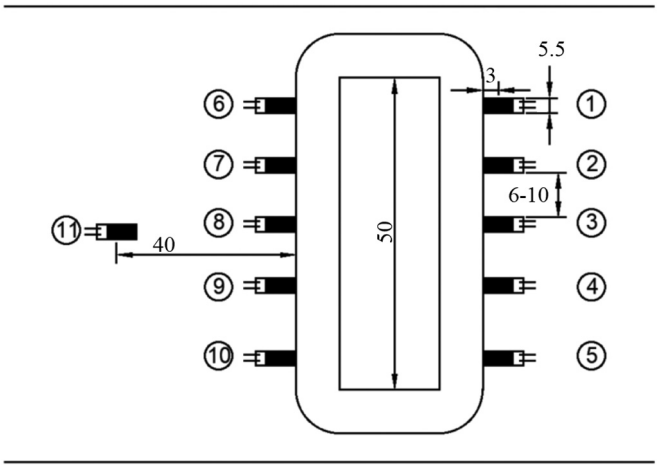

Fig. 3. Strain gauge configuration on test specimen.

by machining their ends with *30°* angle and *0* mm nose to provide better accessibility and reduce the lack of fusion risk. Subsequently, the attachment was tack welded to the base plate, with a gap of *3* mm in order to join them during the subsequent welding runs. Afterward, two subsequent weld runs (root and cap weld) were carried out. The parameters of the weld runs are listed in Table 2, and the welding procedure is shown in Fig. 2.

Before fatigue testing, the specimens were instrumented with several strain gauges at their weld toe to measure the strain drop due to crack initiation as in [15,22–25]. The strain gauges have an overall length and width of *6* and *3* mm respectively. The center of the gauge is placed *3* mm off the weld line. The edge to edge spacing between two adjacent gauges was set to be of around *10 mm*. Moreover, an additional gauge was placed *40* mm off the weld line to measure the membrane stresses. The strain gauge configuration with respect to the attachments is shown in Fig. 3.

2.3. Fatigue test setup

Constant amplitude axial fatigue tests were performed with a stress ratio of *0.29* and a loading frequency of ≈ *30* Hz at the laboratory of *Hamburg University of Technology* (TUHH). The positive stress ratio of 0.29 was chosen in order to simulate the real condition in a bridges where the sustained dead load is taken into account. The testing rig transferred the axial force into the specimens by the means of the hydraulic clamp as shown in Fig. 4. The applied force is measured on the counter side of the force excitation. The specimens were grouped into four series as shown in Table 3. Noticeably, the specimens in series C and D - which are the core of the testing- were tested twice, the first to generate fatigue cracks (Prefatiguing stage), and the latter to investigate the efficiency of the treatments after Prefatiguing stage.

2.4. Supportive investigations

Several auxiliary investigations were conducted to get deeper insight on the treatment's efficiency. The in-depth residual stress distribution was investigated by the hole drilling method. The investigation was conducted on different specimens in as-welded and treated conditions. Besides, a 3D laser scanner was employed to explore the changes in local geometry at the weld toe. Mainly two parameters were studied: weld toe radius and undercut depth. Moreover, Vicker's hardness tester with a test load of *3* kg weight was used. Hardness mapping was performed with a spacing of *0.5* mm in the horizontal and vertical directions. Thus, a metallographic inspection was conducted to ensure the regularity and the adequacy of the fusion depth and to visualize the dominant microstructure before and after treatment. Some specimens were cut and sliced perpendicular to the welding line. The surfaces of the slices were processed by polishing and Nital-etching with *2%* to be prepared for optical microscopy.

Both destructive and non-destructive methods were used to verify and calibrate the use of strain drop measured by attached strain gauges for crack detection for the specimens in series B. Hence, a red dye penetrant was applied to stain the crack surface. Meanwhile, the specimens back walls were scanned continuously by ultrasonic device to identify the crack location and position. Finally, some specimens were cut to monitor the crack profile.

2.5. Crack detection

In addition to the multiple strain gauges, the specimens in series B were scanned by an ultrasonic testing device to inspect the crack depth and dye penetrant was applied to stain the crack surface.

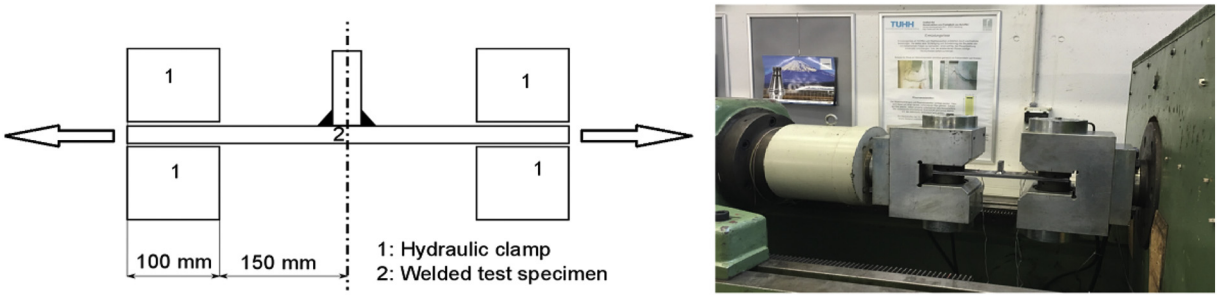

Fig. 4. L: Schematic figure shows the hydraulic clamp. R: Fatigue testing rig.

Table 3
The specimens series.

Series	N.o of spec	Function	Specimens	Test stop criteria
A	12	Constructing the S-N curve for the as-welded	1–10, 12–13	Failure/Run-out
B	3	Crack detection and verification	14–16	50–80% drop in strain
C	7	Studying the life extension by TIG	17–23	Before treatment: 25% drop in strain After treatment: Failure/Run-out
D	5	Studying the life extension by TIG-HFMI	25–29	Before treatment: 25% drop in strain After treatment: Failure/Run-out

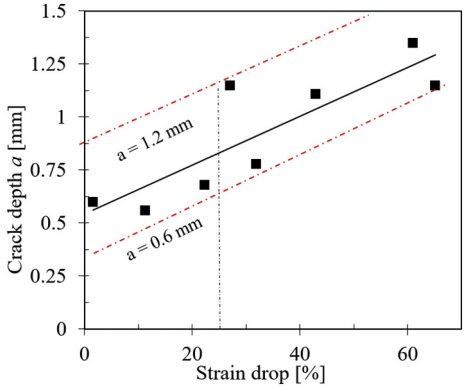

Fig. 5. Crack depth, strain drop correlation.

Afterward, the specimens were opened to monitor to visualize the crack surface. A correlation was found between the strain drop detected by one of the attached strain gauges and the existing crack depth at the weld toe as shown in Fig. 5. Consequently, the specimens in series C and D- which are the testing program- were tested and the abort criterion was set to be *25%* drop in any of the attached strain gauge. This percentage would correspond to a crack size between *0.6* mm and *1.2* mm as shown in the figure. Fig. 6 shows the strain plots against the number of cycles N_f for some specimens in series C and D. Despite the specimens being identical in shape, dimensions, welding and manufacturing method, the prefatigued lives were widely scattered which might be traced back to the intrinsic disparities between the specimens and to the difference in crack initiation location with respect to the strain gauges.

2.6. Crack repair

The welds of the specimens in series C and D were treated by tungsten electrode to melt the toes vicinity. The application of a relatively high heat input ensured deep fusion. The electrode was positioned at the weld toe which thereby created larger undercut at the resulted toe position. However, fitting the electrode at the weld toe secured that the position where maximum fusion was reached corresponded to crack plane. The specimens were clamped from both sides during remelting and they were air-cooled after treating the first side. Then, treating the second side was performed. The heat input were halved at the edges to avoid overheating and subsequent inflammation. The TIG-remelting parameters fall within the recommended ranges as shown in Table 4. The specimens in series D were then HFMI-treated by a single *5* mm radius HiFIT indentor. The angle of inclination of the axis of the indenter with respect to the plate surface was in the range

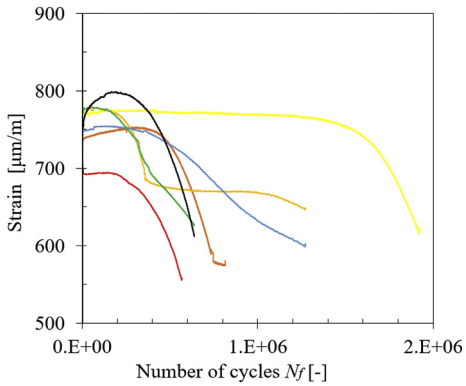

Fig. 6. Examples strain gauge measurements.

Table 4
TIG-remelting parameters.

	Voltage V	Current A	Speed mm/min
In the present study	11.1–12	270–272	100
Recommended by the IIW [3]	12–17	160–250	80–160
	Heat input KJ/mm	Nozzle diameter mm	Electrode diameter mm
In the present study	1.78–1.96	12	3
Recommended by the IIW [3]	1.0–2.5	10–14	3–4

of *60–70*°; this range was recommended when HFMI is to be used for crack retrofitting [20].

3. Results

The as-welded specimens in series A were subjected to different stress ranges between *118* and *175* MPa. The fatigue test results are given in Table 5 and summarized in Fig. 7. Burst fracture of the specimens was set to be the tests abort criterion. However, three specimens ran-out after being subjected to *10* million of cycles. Therefore, the stress ranges were increased to achieve failure within reasonable number of cycles. Notably, the obtained characteristic fatigue strength (FAT) was found to be *125* MPa which is *4* fatigue class higher than the FAT value for transverse attachment stated in the Eurocode [38]. The fatigue strength was estimated by the prediction interval method given by [39]. It is noteworthy that the run-out tests were excluded from the evaluation of the FAT value.

After treatment, the specimens in series C and D showed significant fatigue strength when tested under *150* MPa. Many specimens ran-out after *10* million cycles of loading. Consequently, the loading level was increased to *180* MPa. Nonetheless, some specimens ran-out again after *10* million cycles of loading. Subsequently, the specimens were tested under higher stress levels of *220* or *250* MPa and in all of them fatigue cracks initiated and propagated at the base plate from the clamping location as shown in Fig. 8. Since the specimens were subjected to different stress ranges starting from *150* MPa and ending by *220* or *250* MPa, the equivalent stress ranges $\Delta\sigma_{EQV}$ were used to present the results as in Fig. 7. $\Delta\sigma_{EQV}$ is calculated as follows:

$$\Delta\sigma_{EQV} = \left(\frac{\sum\left(n_j \times \Delta\sigma_j^m\right)}{\sum n_j}\right)^{\frac{1}{m}} \quad (1)$$

where:

$\Delta\sigma_j$: Applied stress range.
j: Applied stress range index.
n_j: Number of cycle at applied stress range $\Delta\sigma_j$.

Table 5
Fatigue tests results of series A (As-welded).

Test	Spec	$\Delta\sigma$ [MPa]	N_f		Test	Spec	$\Delta\sigma$ [MPa]	N_f	
A1a	1	119	10,000,000	RO	A4	4	145	1,080,000	F
A1b	1	143	2,150,000	F	A5	5	175	757,000	F
A2a	2	114	7,850,000	RO	A6	6	170	685,000	F
A2b	2	125	10,400,000	RO	A7	7	165	8,590,000	F
A2c	2	140	8,000,000	RO	A8	8	160	9,870,000	F
A2d	2	132	2,750,000	RO	A9	9	150	1,130,000	F
A2e	2	145	884,000	F	A10	10	150	1,600,000	F
A3a	3	132	2,530,000	RO	A12	12	150	3,250,000	F
A3b	3	139	3,100,000	RO	A13	13	150	2,420,000	F
A3c	3	145	1,080,000	F					

RO: Run-out F: Failure.

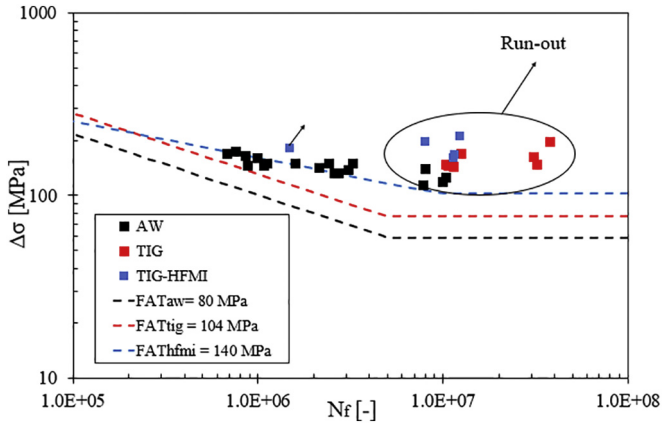

Fig. 7. The fatigue test results of the as-welded and TIG-remelted and TIG-HFMI treated specimens.

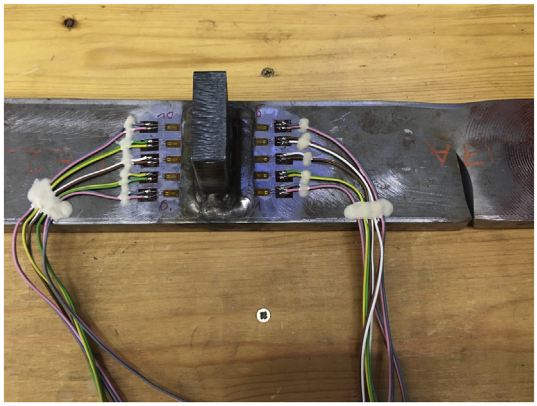

Fig. 8. Fatigue failure in the base metal of the TIG-treated specimen.

m: Presumed slope of the S—N curve (For as-welded and TIG-treated specimen m = *3*, For HFMI-treated specimens m = *5*).

The test results of the specimens in series C and D are given by the red and blue solid rectangles respectively in Fig. 7 and the detailed results of the test are given in Table 6. The S—N curves of these series could not be constructed because they failed at the clamping position. However, the tests showed that all the specimen failures lay above the design S—N curve of the TIG-treated new transverse attachment detail proposed by the IIW recommendation [2]. This indicates the efficiency of the treatment methods in crack retrofitting.

Fig. 9L shows the residual stress distribution measured by the hole drilling method. The measured residual stresses are transversal to the welding line (i.e. parallel to the loading direction). Several holes were drilled in each specimen and the average values were documented; all of them were placed at the same distance of the weld line. Compressive residual stresses were found at the surface even in as-welded specimens. Following the treatment, two remarkable changes could be observed: The compressive stress at the surface became higher and the gradient of the curve became shallower. The combined TIG-HFMI treatment induced further compression as a result of the high indentor's impact energy. Analogous results were found for the local hardness as shown in hardness mapping in Fig. 10.

Vicker's hardness values and the corresponding tensile strength are extracted at the weld toe and plotted in Fig. 9R. Moreover, a significant increase in the weld toe radius was achieved after both of the treatment methods which thereby caused a reduction in stress concentration factor as shown in Fig. 11. However, TIG-remelting caused an increase in the undercut depth; this is traced back to the positioning of the TIG electrode right at the weld toe and not according to the IIW recommendations [3]. The measured toe radii and undercut depth are given in Fig. 12 and Table 7. The table also shows that the scatter of the toe radius became significantly smaller after TIG-remelting.

The regularity and the adequacy of the fusion depth were investigated by a metallographic inspection as mentioned in Section 2.4. In total, 14 slices of the cross-section, cut orthogonal to the weld, were investigated by the optical microscope and an average fusion depth was found to be *2.06* mm with a standard deviation of *0.17* mm. Moreover, the minimum detected fusion depth was *1.36* mm which is larger than the existing crack size (0.6–1.2 mm). This indicates full fusion of the crack surfaces. Moreover, the heat affected zone size was found to be similar for both the MAG-welding and TIG-remelting despite the difference in arc size. This was the result of imposing higher heat input in TIG-remelting than MAG-welding. The inspection showed relatively big pores in the middle of the attachment indicating a lack of fusion. However, no crack was initiated there because of the low stress concentration in this region. All of the aforementioned observations are shown in Fig. 13.

The microscopic constituents of the specimens before and after TIG remelting are shown in Fig. 14. No significant difference was detected between the fusion zone before and after treatment where acicular ferrite was found to be the main constituent. However, Widmanstätten ferrite was detected after TIG-remelting, while islands of allotriomorphic ferrite were found in the weld zone before treatment which might be attributed to the slower cooling rate of the TIG-remelting in comparison to the welding. Besides, Bainite morphology

Table 6
Fatigue test results of the treated specimens.

Test	Spec	Status	Δσ [MPa]	N_f		Test	Spec	Status	Δσ [MPa]	N_f	
A17	17	TIG	150	10,000,000	RO	A22	22	TIG	150	10,000,000	RO
B17	17	TIG	180	10,000,000	RO	B22	22	TIG	250	334,159	CF
C17	17	TIG	110	10,000,000	RO	A23	23	TIG	150	10,000,000	RO
D17	17	TIG	250	2,434,252	CF	B23	23	TIG	250	1,405,626	CF
A18	18	TIG	150	10,800,000	RO	A25	25	TIG-HFMI	220	10,000,000	CF
B18	18	TIG	180	10,000,000	RO	B25	25	TIG-HFMI	250	2,449,821	CF
C18	18	TIG	220	18,000,000	CF	A26	26	TIG-HFMI	180	1,490,000	CF
A19	19	TIG	150	200,000,000	RO	A27	27	TIG-HFMI	150	10,000,000	RO
B19	19	TIG	180	10,331,885	RO	B27	27	TIG-HFMI	220	1,515,187	CF
C19	19	TIG	220	740,910	CF	A28	28	TIG-HFMI	150	10,000,000	RO
A20	20	TIG	150	10,000,000	RO	B28	28	TIG-HFMI	200	1,419,626	CF
B20	20	TIG	220	2,491,395	CF	A29	29	TIG-HFMI	180	5,648,000	RO
A21	21	TIG	150	10,000,000	RO	B29	29	TIG-HFMI	220	2,409,850	CF
B21	21	TIG	250	728,582	CF						

RO: Run-Out CF: Clamping failure.

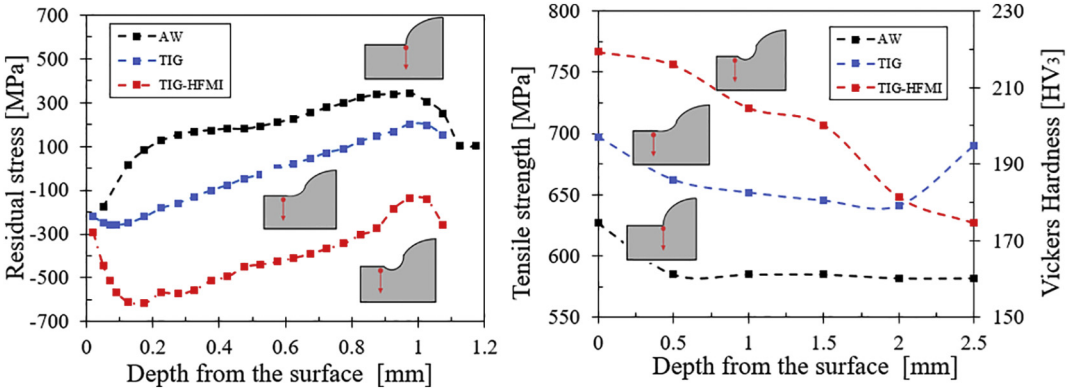

Fig. 9. The In-depth residual stress (Parallel to the loading direction) and the local tensile strength distribution of the as-welded and treated specimens.

dominated in the HAZ of the as-welded specimens and it was tempered after treatment because of the high heat input. The TIG fusion zone which mainly consists of acicular ferrite replaced the heat affected zone in as-welded condition(which consists of bainite) at the weld toe. The interlocking nature of the acicular ferrite, together with its small grain size caused a remarkable increase in the local hardness at the weld toe as shown in Figs. 9 and 14.

The relative displacement of different points along the as-welded specimens was measured so they could be compared to the corresponding points after treatment as shown in Fig. 15. The TIG-remelting caused additional distortions in the longitudinal direction and twisting the specimens in the transverse direction. This caused a divergence of the two curves corresponding to TIG-remelting in Fig. 15. The high distortion was caused by the high heat input used to achieve deep fusion.

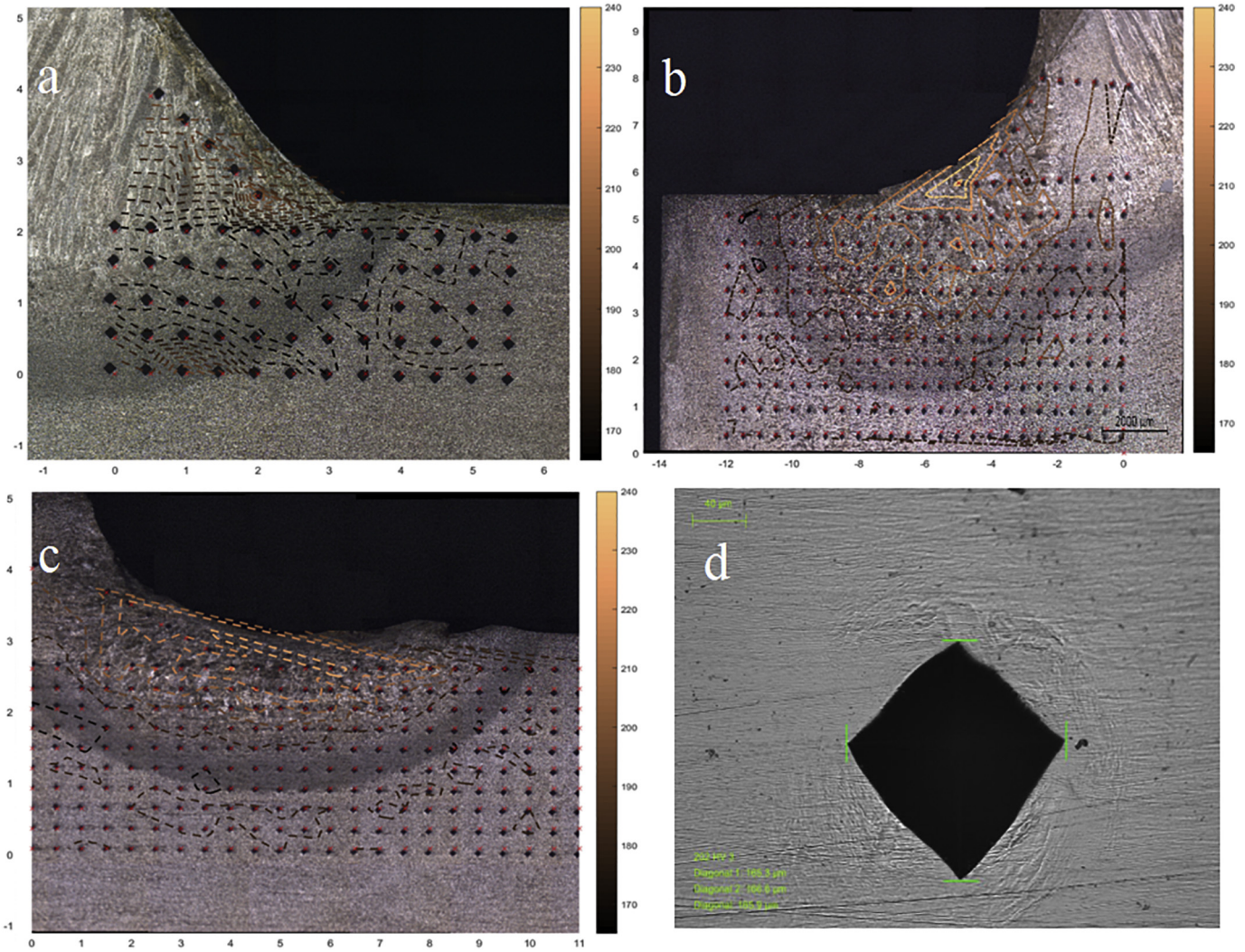

Fig. 10. The hardness distribution in the vicinity of the weld in: a:as-welded b:TIG-treated c:TIG-HFMI treated d: Vicker's hardness indent sample.

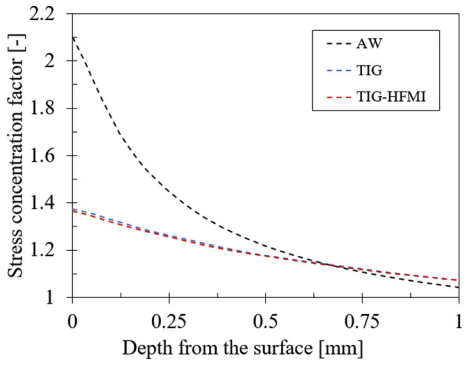

Fig. 11. The elastic stress concentration factor.

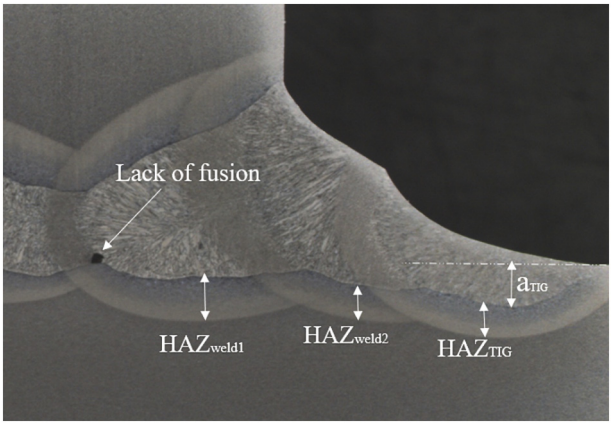

Fig. 13. Microscopic investigation of the weldment after TIG remetling.

On the other hand, TIG-HFMI treated specimens in series D were less distorted than TIG-treated specimens in series C because of the applied constraint on the specimen when HFMI treated.

4. Discussion

The as-welded specimens showed a remarkably long fatigue life as mentioned in the previous section. This might be explained by the presence of compressive residual stress at the weld toe as shown in Fig. 9. On the other hand, straightening of the distorted specimens upon clamping by the test machine would give rise to tensile mean stress at the weld toe which counteracts the effect of compressive residual stress. In light of that, the relation between the angular distortion and the clamping stress was studied thoroughly. The clamping stresses were evaluated experimentally by the attached strain gauge *40* mm away from the weld line (i.e. SG 11 shown in Fig. 3). The expected correlation between the clamping stress and the angular distortion was found, see Fig. 16.

Since the clamping stresses were derived from the strain measurement 40 mm of the welds, the local stress at the weld toe could not be directly obtained. Therefore, a linear elastic 2D finite element analysis was conducted using the commercial software ABAQUS/CAE2017 to evaluate the local stress due to clamping. In order to eliminate the stress singularity, a toe radius of 1 mm was used in accordance with the IIW recommendation regarding the effective notch approach [2]. *4*-noded bi-linear plane stress elements (CP4SR in Abaqus notation) were used to create the mesh and a convergence study for the mesh size led to an element size of 0.025 mm in the weld toe vicinity and *2* mm elsewhere.

Several models were created with several specimen's geometries based on the measured angular distortions. The elasticity modulus and Poisson's ratio are chosen to be 210 GPa and 0.3 respectively. The clamping jaws were simulated as solid undeformed bodies approaching

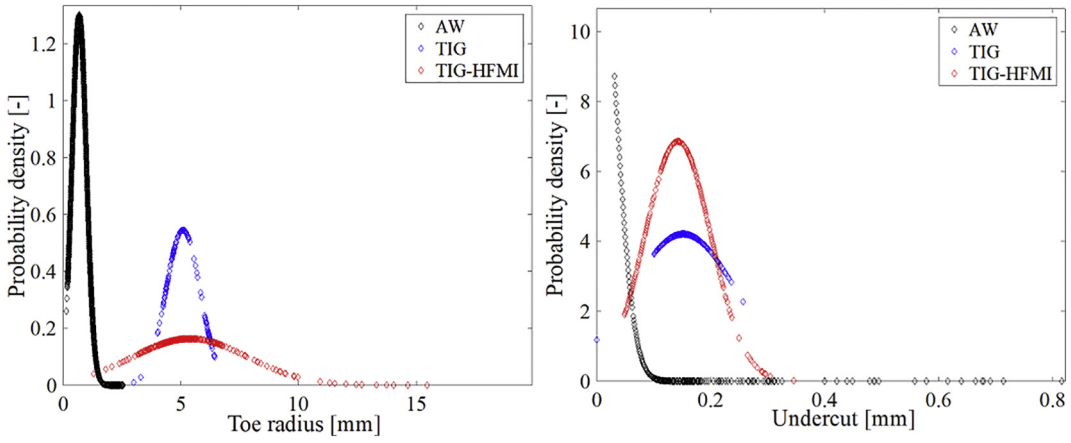

Fig. 12. The weld toe radius and undercut height normal distributions before and after treatment.

Table 7
The geometrical parameters of the tested specimens before and after treatments.

Status	AW		TIG		TIG-HFMI	
The geometrical parameter	Toe radius	Undercut	Toe radius	Undercut	Toe radius	Undercut
Mean	0.67 mm	0.004 mm	5.09 mm	0.150 mm	5.39 mm	0.14 mm
Standard deviation	0.31 mm	0.03 mm	0.73 mm	0.10 mm	2.44 mm	0.06 mm
Variation coefficient	0.46	8.74	0.14	0.67	0.45	0.41
Population size	20,660	20,660	150	1581	334	351

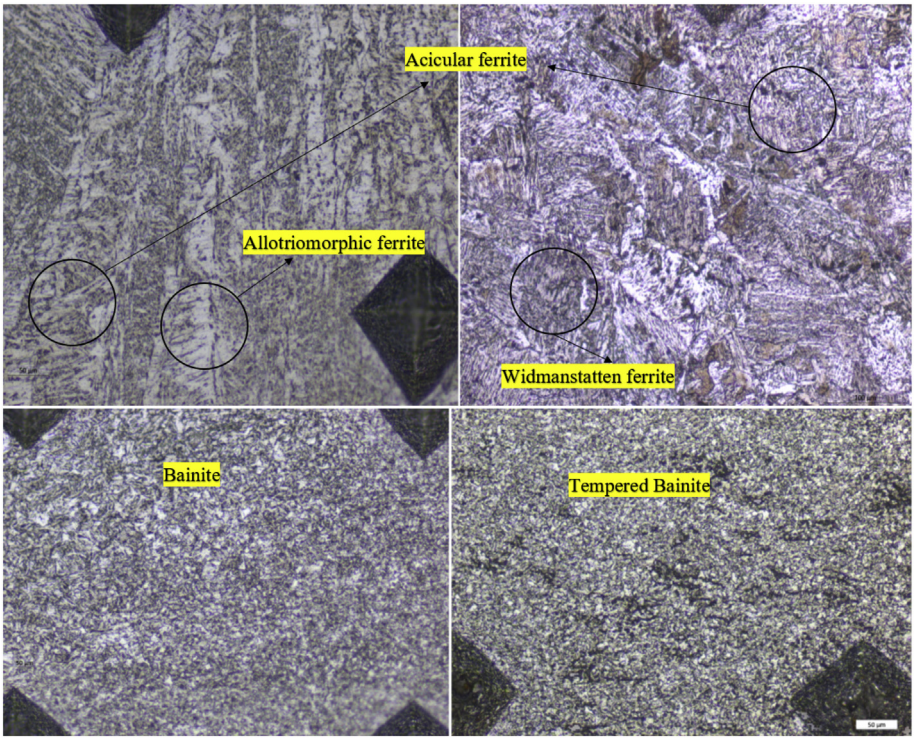

Fig. 14. Micrographic picture for the fusion zone (Top) and heat affected zone (Bottom) before and after TIG-remelting.

each other in a displacement control manner (i.e. vertical displacement was predefined). The displacement of the jaws was restricted in the horizontal direction ($u_x = 0$). Besides, hard normal contact was defined between the clamping jaws (i.e. the master surface) and the specimen (i.e. the slave surface). Subsequently, the results were extracted when the specimen got fully straightened and the inclination of the specimen's wings became zero. The model results are shown in Fig. 17.

The obtained nominal stresses were extracted at the location of the strain gauges (*40* mm of the weld line). The model was validated by comparing them against the experimentally obtained nominal stresses and the differences were found to be insignificant as shown in Fig. 16. Subsequently, the local stress at the notch was obtained along the weld toe. The average angular distortion in as-welded condition of *0.26* corresponds to local clamping stress of *90* MPa which is thereby less than the existing compressive residual stresses of *−176* MPa.

Despite the long fatigue life obtained for the as-welded specimens, both treatment methods resulted in significant fatigue lives extension. That is conspicuous in Fig. 7 where the solid red and blue rectangles (TIG, TIG-HFMI respectively) are located to the top of the black rectangle (AW). The successful fatigue life extension by the treatment can be explained by the shallowness of the existing crack and the efficiency of the treatment in terms of local geometry improvement, residual stress change, and local material hardening. The combined effects of these three factors could be grasped by Goodman's mean stress correction given in Eq. (5).

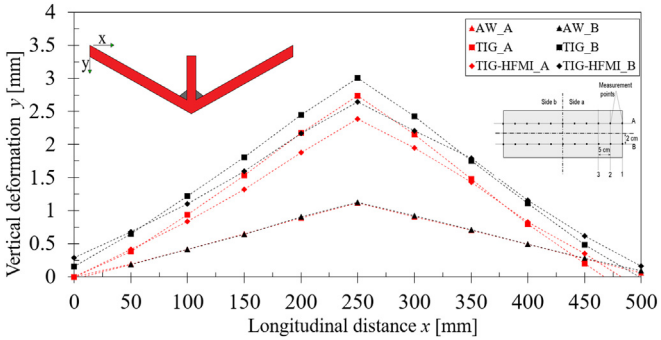

Fig. 15. The distortion of the specimens before and after treatments.

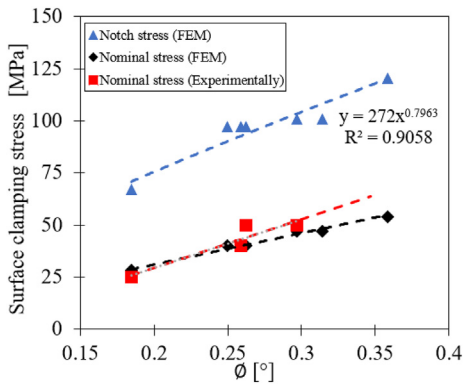

Fig. 16. The correlation between the angular distortion and the clamping stress.

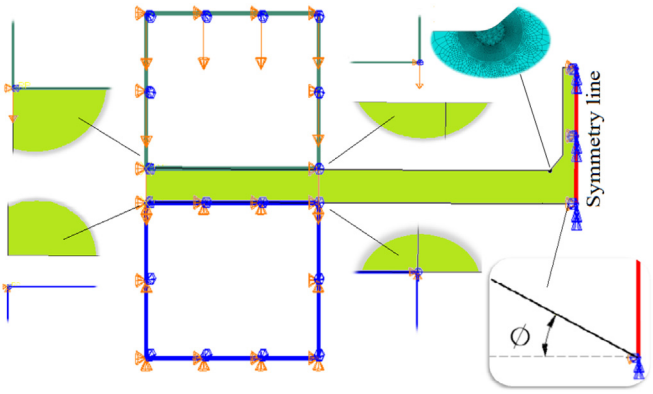

Fig. 17. The finite element model for simulating the clamping process.

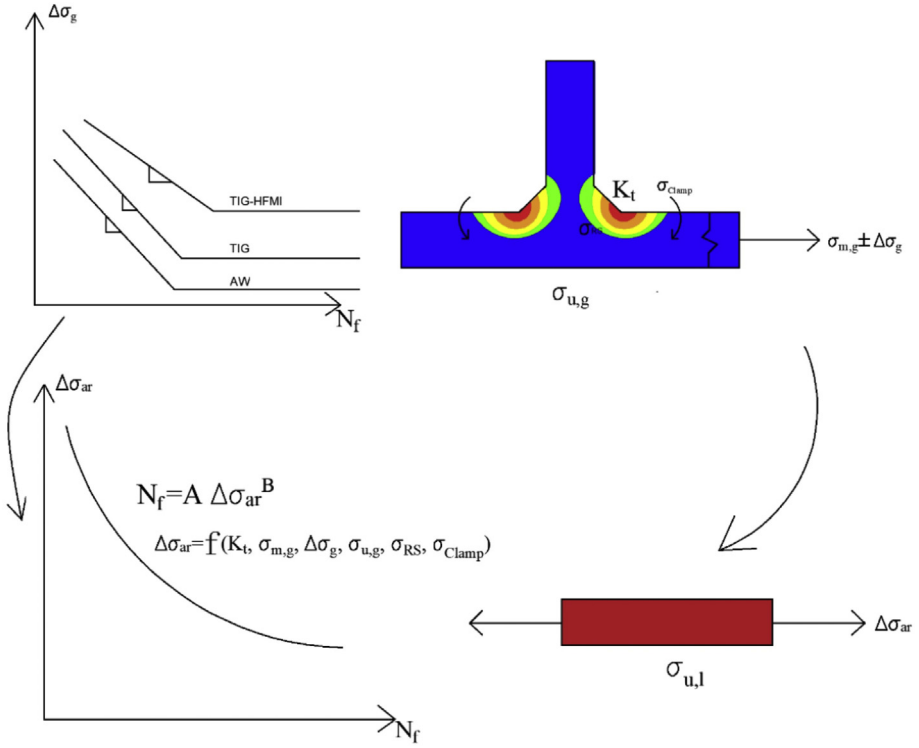

Fig. 18. Incorporation of different factors to evaluate the fatigue life locally.

Basquin's Equation is a power-law relationship which describes the linear relationship between the applied stress range ($\Delta\sigma_{ar}$) and the number of cycles to failure (N_f) plotted in a log-log scale, see Eq. (6). Basquin's equation's constants for S355 steel (A and B) were obtained from [37]. Since the mean stresses (i.e. axial mean stress, residual stress and clamping stress) and the measured local ultimate strength were taken into account, the S—N curve of the base metal could be used instead of separate S—N curves for as-welded, TIG-dressed and TIG-HFMI treated details. This concept is illustrated in Fig. 18.

The calculated fatigue life $N_{g,\,calc}$ using Eqs. 2, 3, 4, 5 and 6 are compared to the test results for as-welded and treated specimens $N_{f,\,exp}$. See Table 8. The stresses are given in MPa in the table. The calculated as-welded fatigue life under a stress range of 150 MPa was found to be around 2.61 million cycles which lies in the interval of the obtained experimentally determined fatigue lifes (1.11–3.25 million cycles) under the same stress range. In addition, most of the test results confirmed the model predictions for the treated specimens' lives since no toe failure was obtained when the specimens were tested to $N_{f,\,exp}$ as shown in the table. Nonetheless, Basquin's Equation should not be used when the fully reversed stress range is greater than the local tensile strength of the material $\sigma_{u,\,l}$. Therefore, no predictions were made when $\Delta\sigma_{ar} > \sigma_{u,\,l}$.

$$\Delta\sigma_l = K_t \times \Delta\sigma_g \tag{2}$$

$$\sigma_{m,l} = K_t \times \sigma_{m,g} \tag{3}$$

$$\sigma_{m,tot} = \sigma_{m,l} + \sigma_{RS} + \sigma_{Clamp} \tag{4}$$

$$\Delta\sigma_{ar} = \frac{\Delta\sigma_l}{1 - \frac{\sigma}{\sigma_{u,l}}} \tag{5}$$

$$N_{f,cal} = A \times \Delta\sigma_{ar}^{B} \tag{6}$$

where $\Delta\sigma_{ar}$ is the fully reversed stress range considering the mean stress, while $\Delta\sigma_l$ and $\Delta\sigma_g$ are the local and global stress ranges respectively. The global and local mean stresses due to external loading are denoted in the equations by $\sigma_{m,\,g}$ and $\sigma_{m,\,l}$ respectively. The additional mean stresses due to residual stress σ_{RS} and clamping stress σ_{Clamp} were obtained from the distributions shown in Figs. 9 and 16 respectively. Besides, the local tensile strength at the weld toe and the ultimate strength of S355 structural steel are given in the equations as $\sigma_{u,\,l}$ and $\sigma_{u,\,g}$

Table 8
Calculated fatigue lives for as-welded and treated specimens under different loading levels.

	σ_{RS}	$\sigma_{u,\,l}$	σ_{Clamp}	$\sigma_{m,\,g}$	$\Delta\sigma_g$	K_t	$\sigma_{m,\,l}$	$\sigma_{m,\,tot}$	$\Delta\sigma_l$	$\Delta\sigma_{ar}$	$N_{f,\,cal}$	$N_{f,\,exp}$
AW	−176	627	90	136	150	2.150	292	206	323	481	2.61E6	1.11E6–3.25E6
TIG	−219	697	198	136	150	1.366	186	165	205	279	1.16E9	1.0E7
TIG-HFMI	−293	767	171	136	150	1.360	185	62	204	268	1.79E9	1.0E7
AW	−176	627	90	162	180	2.150	348	262	387	665	–	–
TIG	−219	697	198	162	180	1.366	221	200	246	345	1.08E8	1.0E7
TIG-HFMI	−293	767	171	162	180	1.360	222	98	245	281	1.10E9	1.50E6
AW	−176	627	90	200	220	2.150	430	334	473	1047	–	–
TIG	−219	697	198	200	220	1.366	275	252	300	470	3.29E6	–
TIG-HFMI	−293	767	171	200	220	1.360	273	150	299	371	4.66E7	1.50E6
AW	−176	627	90	227	250	2.150	488	402	537	1499	–	–
TIG	−219	697	198	227	250	1.366	310	289	341	583	3.01E5	3.30E5
TIG-HFMI	−293	767	171	227	250	1.360	308	186	340	450	5.56E6	2.40E6

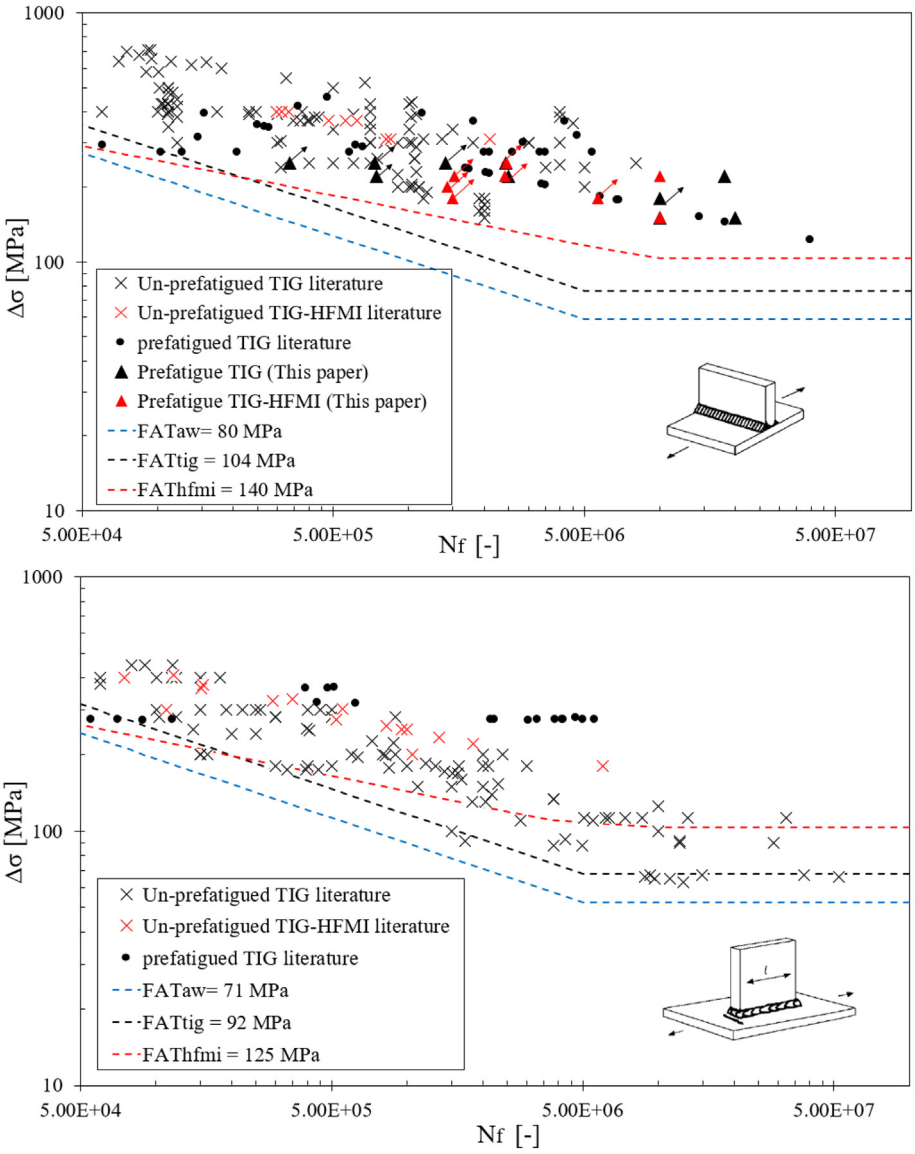

Fig. 19. Fatigue test results of TIG and TIG-HFMI treated transverse and longitudinal attachments respectively.

respectively. The stress concentration factor at the weld toe K_t were obtained from Fig. 11.

Several fatigue test results of TIG-treated and TIG-HFMI treated transverse and longitudinal attachment specimens were collected from the literature [7,9,14,15,17,32,33,40–42] and are presented in Fig. 19. No distinction was made based on the failure position, mean stress, stress ratio or plate thickness. The fatigue test results of the treated specimens —In this paper- are denoted by the black and red triangles in the figure. The characteristic S—N curve of the as-welded, TIG-dressed and HFMI-treated specimens are also shown in the figure.

For transverse attachments, more than 98% of the collected data points exhibited longer fatigue life than the characteristic life for new TIG-treated attachment (i.e. Un-prefatigued) given in the IIW [2] at the same stress range. The only two points lying below the line are referred to prefatigued specimens containing deep crack at the weld toe (deeper than 5 mm). Otherwise, the rest of the prefatigued specimens (Including the tested ones in this paper) are lying within the scatter band of the new ones (i.e. Un-prefatigued ones). The resistance of the longitudinal attachments was found to be more scattered because of its dependency on the attachment length. However, the prefatigued specimens showed relatively long fatigue lives with an exception for specimens containing relatively deep crack (deeper than 5 mm). This indicates the successful application of TIG-remelting in fatigue crack retrofitting.

The combined effect of TIG-dressing followed by HFMI-treatment has - to the best of the authors' knowledge - never been investigated as crack retrofitting technique. However, it was reported in the literature that it can be used to strengthen new welded structures [40]. Though the tested specimens in this paper did not fail at the weld toe, their fatigue lives were long as shown in Fig. 19 and lying way above the design curve of the TIG-treatment for this detail. Despite that the local stress range for the TIG-HFMI treated specimens is lower than TIG-treated ones as shown in Table 8, no quantitative comparison could be made between the tested TIG'ed. and TIG-HFMI'ed. specimens because none of them failed at the weld toe.

5. Conclusions

Fatigue tests were carried out on S355 structural steel plates with welded transverse attachment to investigate the performance of two post-weld treatment methods (TIG-remelting, TIG-HFMI treatment) in fatigue crack retrofitting. A crack detection methodology was applied

based on strain drop. Several auxiliary investigations were carried out to give deeper insight on treatment effects. The following conclusion can be drawn:

- The as-welded fatigue life was found to be relatively long which is mainly attributed to the presence of compressive residual stress at the weld toe.
- No remarkable difference was observed in the microstructure of the fusion zone after welding and re-melting and the same applies to the heat-affected zone.
- Both treatment methods caused a substantial change in the local weld topography where the toe radius increased with a factor of *7*.
- Despite the compressive residual stress found in the as-welded state, TIG-remelting caused a further increase in the compressive stresses at the surface and a decrease in the stress distribution gradient. HFMI-treatment induced further compression at the weld toe.
- TIG-remelting caused an increase in the hardness value at the weld toe since the heat-affected zone was replaced by a TIG fusion zone with an acicular microstructure. The HFMI treated zone experienced further local hardening because of the cold working effect.
- A correlation was found between the clamping stresses and the angular distortions. Besides, a good match was found between the finite element results and the experimentally measured clamping stresses. TIG-remelting increased the distortions while HFMI-treatment reduces them.
- A significant increases in fatigue lives was obtained by both of the investigated treatment methods. Thereby, many specimens ran-out after 10 million cycles when subjected to membrane stress range of *150* MPa.
- When the treated specimens were tested at stress level larger than 150 MPa, base metal failures from the clamping position were observed. This emphasizes the strength of weld toe position after TIG-remelting in case of full crack removal.
- The effect of strain hardening, geometry improvement, residual and clamping stresses were combined using Goodman mean stress correction and Basquin's Equations. Long fatigue lives were obtained which explained the results from the experiments. The calculated fatigue lives were found to be in line with the test results.
- The combined effect of TIG-remelting and HFMI-treatment found to be more effective in fatigue life extension than TIG-remelting. However, this could not be verified by fatigue testing as no failure at the weld toe was obtained.

Declaration of Competing Interest

The authors declare that they have no known competing financial interests or personal relationships that could have appeared to influence the work reported in this paper.

Acknowledgments

The authors are grateful to the road administration (*Trafikverket*) and the innovation system agency in Sweden *Vinnova* (*Infra Sweden 2030*) who financed the whole project. Gratitude is also directed to Nils Fredrich from Hamburg University of Technology and for Dr. Mattias Thuvander from Chalmers University of Technology who contributed generously in fatigue testing, residual stress measurements, and microscopy.

References

[1] Z. Barsoum, Henry granjon prize competition 2010 winner category C:"design and structural integrity" fatigue design of welded structures—some aspects of weld quality and residual stresses, Welding World 55 (11–12) (2011) 2–11.
[2] A. Hobbacher, Recommendations for fatigue design of welded joints and components. IIW document xiii-2151–07, XV-1254r1–07, Paris 2007 (2007).
[3] P. Haagensen, S. Maddox, IIW recommendations on post weld improvement of steel and aluminium, IIW Doc 13 (2003)1815–00.
[4] P. Haagensen, et al., TIG Dressing of Steel Weldments for Improved Fatigue Performance, 1979.
[5] L.C. Wu, D.P. Wang, Improve the fatigue performance of welded joints with undercuts by TIG dressing treatment, 472, 2012 1300–1304.
[6] H. Mettänen, et al., Fatigue strength assessment of TIG-dressed ultra-high-strength steel fillet weld joints using the 4R method, Int. J. Fatigue (2020) 105745.
[7] H.C. Yldrm, Review of fatigue data for welds improved by tungsten inert gas dressing, Int. J. Fatigue 79 (2015) 36–45.
[8] S. Van Es, M. Kolstein, R. Pijpers, F. Bijlaard, TIG-dressing of high strength butt welded connections–part 2: physical testing and modelling, Procedia Eng. 66 (2013) 126–137.
[9] M.M. Pedersen, O.Ø. Mouritsen, M.R. Hansen, J.G. Andersen, J. Wenderby, Comparison of post-weld treatment of high-strength steel welded joints in medium cycle fatigue, Welding World 54 (7–8) (2010) R208–R217.
[10] S. Van Es, M. Kolstein, R. Pijpers, F. Bijlaard, TIG-dressing of high strength steel butt welded connections–part 1: weld toe geometry and local hardness, Procedia Eng. 66 (2013) 216–225.
[11] M. Nascimento, H.J.C. Voorwald, J.D.C.P. Filho, Effects of several TIG weld repairs on the axial fatigue strength of aisi 4130 aeronautical steel-welded joints, Fatigue Fract. Eng. Mater. Struct. 35 (3) (2012) 191–204.
[12] H. Lieurade, I. Huther, F. Lefebvre, Effect of weld quality and postweld improvement techniques on the fatigue resistance of extra high strength steels, Welding World 52 (7–8) (2008) 106–115.
[13] L. Huo, D. Wang, Y. Zhang, Investigation of the fatigue behaviour of the welded joints treated by TIG dressing and ultrasonic peening under variable-amplitude load, Int. J. Fatigue 27 (1) (2005) 95–101.
[14] C. Miki, T. Mori, S. Tuda, K. Sakamoto, Retrofitting fatigue-cracked joints by TIG arc remelting, Doboku Gakkai Ronbunshu 1987 (380) (1987) 111–119.
[15] A.L. Ramalho, J.A. Ferreira, C.A. Branco, Fatigue behaviour of T welded joints rehabilitated by tungsten inert gas and plasma dressing, Mater. Des. 32 (10) (2011) 4705–4713.
[16] J.W. Fisher, A.W. Pense, R.E. Slockbower, H. Hausammann, Retrofitting fatigue damaged bridges, Transp. Res. Rec. (664) (1978).
[17] H. Al-Karawi, A. Manai, M. Al-Emrani, R. Von Bock, N. Friedrich, J. Hedegård, Fatigue crack repair by TIG-remelting, The International Conference on Bridge Maintenance, Safety and Management IABMAS (submitted and accepted), Sapporo, Japan, 2020.
[18] J. Fisher, M. Sullivan, A. Pense, Improving fatigue strength and repairing fatigue damage, Final Report, NCHRP Project 1974, pp. 12–15.
[19] J. Baumgartner, H.C. Yldrm, Z. Barsoum, Fatigue strength assessment of TIG-dressed welded steel joints by local approaches, Int. J. Fatigue 126 (2019) 72–78.
[20] H. Al-Karawi, J. Al-Emrani, Mohammadand Hedegård, Crack behaviour after high frequency mechanical impact treatment in welded S355 structural steel, The International Conference on Bridge Maintenance, Safety and Management IABMAS (Submitted and Accepted), Sapporo, Japan, 2020.
[21] S.J. Maddox, M. Doré, S.D. Smith, A case study of the use of ultrasonic peening for upgrading a welded steel structure, Welding World 55 (9–10) (2011) 56–67.
[22] A. Akyel, M. Kolstein, F. Bijlaard, Fatigue strength of repaired welded connections made of very high strength steels, Eng. Struct. 161 (2018) 28–40.
[23] A. Akyel, M. Kolstein, F. Bijlaard, Fatigue strength of repaired cracks in base material of high strength steels, J. Constr. Steel Res. 139 (2017) 374–384.
[24] M. Leitner, Z. Barsoum, F. Schäfers, Crack propagation analysis and rehabilitation by HFMI of pre-fatigued welded structures, Welding World 60 (3) (2016) 581–592.
[25] C. Branco, V. Infante, R. Baptista, Fatigue behaviour of welded joints with cracks, repaired by hammer peening, Fatigue Fract. Eng. Mater. Struct. 27 (9) (2004) 785–798.
[26] V. Infante, C. Branco, A study on the fatigue behaviour of damaged welded joints repaired by hammer peening, *ECF13,* San Sebastian, 2000, , 2000.
[27] K. Houjou, K. Takahashi, K. Ando, H. Abe, Effect of peening on the fatigue limit of welded structural steel with surface crack, and rendering the crack harmless, Int. J. Struct. Integr. 5 (4) (2014) 279–289.
[28] R. Fueki, K. Takahashi, Prediction of fatigue limit improvement in needle peened welded joints containing crack-like defects, Int. J. Struct. Integr. 9 (1) (2018) 50–64.
[29] Y. Kudryavtsev, J. Kleiman, A. Lugovskoy, L. Lobanov, V. Knysh, O. Voitenko, G. Prokopenko, Rehabilitation and repair of welded elements and structures by ultrasonic peening, Welding World 51 (7–8) (2007) 47–53.
[30] H.-P. Günther, U. Kuhlmann, A. Dürr, Rehabilitation of welded joints by ultrasonic impact treatment (UIT), IABSE Symposium Report, vol. 90, International Association for Bridge and Structural Engineering 2005, pp. 71–77.
[31] R. Fueki, K. Takahashi, K. Houjou, Fatigue limit prediction and estimation for the crack size rendered harmless by peening for welded joint containing a surface crack, Mater. Sci. Appl. 6 (06) (2015) 500.
[32] T. Skriko, M. Ghafouri, T. Björk, Fatigue strength of TIG-dressed ultra-high-strength steel fillet weld joints at high stress ratio, Int. J. Fatigue 94 (2017) 110–120.
[33] P. Haagensen, et al., Tig dressing of steel weldments for improved fatigue performance, Offshore Technology Conference, Offshore Technology Conference, 1979.
[34] H. Alkarawi, A. Manai, M. Al-Emrani, Fatigue Life Extension of Welds: A Critical View on the State of the Art, Chalmers university of technology publications, 2019.
[35] N. Standard, Material data sheets for structural steel, Norway Technology Center, *N-0306 Oslo*, Norway, 2000.
[36] ESAB, Coreweld C6LF, https://www.esabna.com/us/en/products/filler-metals/metal-cored-wires-mcaw/mild-steel-wires/coreweld-c6-lf.cfm.
[37] A.M. de Jesus, R. Matos, B.F. Fontoura, C. Rebelo, L.S. da Silva, M. Veljkovic, A comparison of the fatigue behavior between S355 and S690 steel grades, J. Constr. Steel Res. 79 (2012) 140–150.

[38] E. C. for Standardization, Eurocode 3: Design of steel structures. part 1.9: Fatigue, 2003.
[39] N. Powers, D.M. Frangopol, R. Al-Mahaidi, C. Caprani, Maintenance, safety, risk, management and life-cycle performance of bridges, Melbourne, Australia, Proceedings of the Ninth International Conference on Bridge Maintenance, Safety and Management, 2018.
[40] E.S. Statnikov, V. Muktepavel, A. Blomqvist, Comparison of ultrasonic impact treatment (UIT) and other fatigue life improvement methods, Welding World 46 (3–4) (2002) 20–32.
[41] P. Haagensen, E.S. Statnikov, L. Lopez-Martinez, Introductory fatigue tests on welded joints in high strength steel and aluminium improved by various methods including ultrasonic impact treatment (UIT), IIW Doc 13 (1998) 1748–1798.
[42] L.L. Martinez, A. Blom, H. Trogen, T. Dahle, Fatigue behaviour of steels with strength levels between 350 and 900 MPa influence of post weld treatment under spectrum loading, in: A.F. Bloom (Ed.), Proceeding of the North European Engineering and Science Conference,(NESCO), Welded High-Strength Steel Structures, Stockholm, London, EMAS Publishing, 1997.